IEEE Access
Multidisciplinary | Rapid Review | Open Access Journal

Received January 16, 2018, accepted March 4, 2018, date of publication March 12, 2018, date of current version April 18, 2018.

Digital Object Identifier 10.1109/ACCESS.2018.2814593

Frequency-Distinct Control of Wind Energy Conversion System Featuring Smooth and Productive Power Output

FENG JIA[1,2], XU CAI[1,2], AND ZHENG LI[3]

[1]School of Electronic Information and Electrical Engineering, Shanghai Jiao Tong University, Shanghai 200240, China
[2]Wind Power Research Center, Shanghai Jiao Tong University, Shanghai 200240, China
[3]College of Science and Technology, Donghua University, Shanghai 201620, China

Corresponding author: Xu Cai (xucai@sjtu.edu.cn)

This work was supported by the National Natural Science Foundation of China under Grant 51677117.

ABSTRACT Improving maximum power point tracking ability (MPPTA) and smoothing electric power fluctuation (EPF) are two important goals for optimizing wind power generation. Sufficient works have been done on both goals separately, but the multi-objective optimization of wind energy conversion system (WECS) is lack of theoretical analysis. In this paper, the small signal analysis method is applied to get a frequency-domain declaration for both MPPTA and EPF. The analysis results show when applying traditional optimal torque control (OTC), a larger moment of inertia of WECS is preferred for smoothing EPF, while a smaller moment of inertia is preferred for improving MPPTA, i.e., the two optimization goals contradict with each other. Furthermore, the existing control strategies for improving MPPTA are summarized as virtual-inertia embedded OTC, which turns out to have adverse impacts on EPF. To simultaneously optimize these two contradictory goals, a novel frequency-distinct optimal torque control approach is proposed, and a novel criterion for evaluating MPPTA is presented to facilitate controller parameter design. The analysis results and the proposed control strategy are fully verified by refined co-simulation platform based on GH Bladed and real time digital simulator.

INDEX TERMS Wind power generation, frequency domain analysis, maximum power point tracking, power fluctuation, small signal analysis.

I. INTRODUCTION

Wind power has been one of the most promising renewable energies [1]. However, there are also many challenges for wind energy conversion system (WECS). These challenges include lowering the levelized cost of energy (LCOE) continuously [2] and adapting to grid-friendly requirements [3], among them, improving power production and power smoothing are two important optimization goals for WECS.

Lots of researches have been done on maximum power point tracking of WECS. The basic methods for tracking optimal operating point (OOP) are perturb and observe (P&O) control (P&O is also known as hill-climbing searching control), tip speed ratio (TSR) control, optimal torque control (OTC) and power signal feedback (PSF) control [4]–[7]. Nowadays, the advanced controls, such as fuzzy control [8] and sliding mode control [9] are also introduced in WECS control. The comparison study in [10] shows OTC outperforms TSR in terms of power fluctuation and mechanical loads. OTC is widely adopted by MW-scale WECS because of its simplicity and good performance [11], [12]. As the moment of inertia of MW-scale WECS is large, the maximum power point tracking ability (MPPTA) is weak. So another research point is focused on enhancing MPPTA [12]–[16], among which, [12] takes flexible shaft into consideration, whereas [14] proposed a constant-bandwidth tracking strategy.

Another problem worth attention is the electric power fluctuation (EPF) caused by randomness and intermittent nature of natural wind. The EPFs of large scale wind farm may affect the frequency stability of power grid [17], [18]. In the distributed integration application where the grid strength is rather weak, EPF may have severe adverse impacts on voltage stability [19]. One way to smooth the EPF is to cut the peak of aerodynamic power captured by wind turbine through power curtailment control [20], however, this may considerably lose

power production. Another way to smooth the EPF is to phase shift the electric power through peak cutting and valley filling with the aid of energy storage system (ESS). Extra ESSs have been used for smoothing EPF [21], [22], but the high cost limits its applications. Some other power smoothing schemes utilize the moment of inertia of wind turbine [23], [24]. A power smoothing scheme with rotor-speed-dependent gain has been proposed in [23], and a new control structure has been proposed to make wind turbine appear as adjustable power filters [24], and the limits on power smoothing has been quantified in [25].

Yet most works are focused on only one optimization goal. The simulation and experimental results in [15] shows enhancing MPPTA may cause excess EPFs. Taking both optimization goals into consideration, the power smoothing scheme in [26] still cause little power loss, and the MPPTA enhancement in [27] still cause larger EPFs than conventional OTC. Through theoretical analysis, this paper reveals the two optimization goals are irreconcilable when applying the existing control strategies. Then a frequency-distinct OTC approach is proposed to work out both goals, and the method for designing parameters is given.

II. MAXIMUM POWER POINT TRACKING ABILITY AND POWER SMOOTHING ANALYSIS

Taking WECS as a whole, wind speed is the most important external input. The transfer function from fluctuating wind speed to fluctuating electric power $\Delta P_e(s)/\Delta v(s)$ can be used to describe power fluctuation caused by wind speed variations. The essence of maximum power point (MPP) tracking is to keep the wind turbine operating on optimal tip speed ratio λ_{opt}, which means a certain ratio between generator speed and wind speed. Thus the transfer function from fluctuating wind speed to varying rotor speed $\Delta\omega(s)/\Delta v(s)$ can be used to describe the MPPTA.

In literatures, the amplitude-frequency response (AFR) of $\Delta P_e(s)/\Delta v(s)$ is used to evaluate the power fluctuation character (the lower AFR, the smoother power), and without concern on the phase-frequency response (PFR) [18]. This is reasonable as the phase relation between P_e and random v is meaningless. Similarly, the AFR of $\Delta\omega(s)/\Delta v(s)$ is used to evaluate the MPPTA [15]. However, the phase lag between rotor speed and wind speed also cause a tracking error to λ_{opt}, as illustrated in Fig. 1. So the PFR of $\Delta\omega(s)/\Delta v(s)$ should be considered together with the AFR to evaluate the MPPTA.

According to the Van de Hoven spectrum of natural wind [28], wind fluctuations above 0.5 Hz seldom exist or contain tiny energy, so this paper set 0.5 Hz as the upper limit of the frequency band we are interested in. The dominant mode of torsional vibration is usually 1.5 to 3 Hz, so it is reasonable to simplify the analysis with the lumped-mass drive train model. It is beneficial to work out the key factors, and the analysis results will be validated by simulations with detailed model.

To make the analysis method suitable for both direct-driven WECS and geared WECS, it is necessary to per unit the power

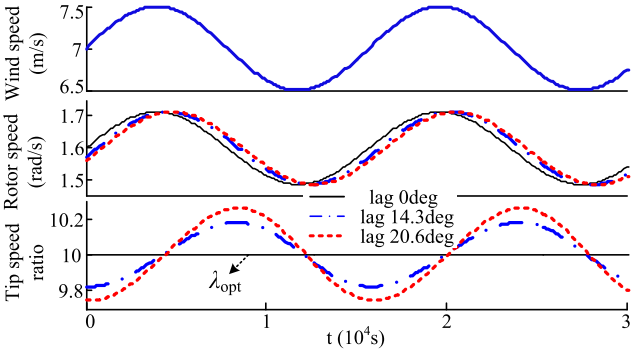

FIGURE 1. Impacts of rotor speed phase lag on MPPTA.

train variables. Set P_B and ω_B as the base power and the base rotational speed of wind turbine, the base speed of generator is $n_{gb}\omega_B$ (n_{gb} is the gear ratio, $n_{gb} = 1$ for the direct-drive WECS). The per-unit inertia of the lumped mass of WECS is

$$J_{sum} = J_{WT}/(P_B/\omega_B^2) + J_G/[P_B/(\omega_B n_{gb})^2] \tag{1}$$

where J_{WT} and J_G are the actual inertia of wind turbine and generator. Take ω as the p.u. speed of lumped mass, the motion equation (ignoring losses) is

$$J_{sum}\dot{\omega} = T_a - T_e \tag{2}$$

where T_a and T_e are per unit aerodynamic torque and generator torque. For the DFIG-based WECS in this paper, P_B is set to the rated power P_n, the base speed of generator is set to the synchronous speed of DFIG. Multiple ω on both side of (2) and linearize it,

$$J_{sum}\omega_0 \mathrm{d}\Delta\omega/\mathrm{d}t = \Delta P_a - \Delta P_e. \tag{3}$$

The per unit aerodynamic power is

$$P_a = k_a v^3 C_p(\lambda, \beta) \tag{4}$$

where $k_a = 0.5\rho\pi R^2/P_B$, ρ is air density, v is wind speed, R is rotor diameter, λ is tip speed ratio, β is pitch angle.

$$\lambda = \omega_B \omega R/v. \tag{5}$$

Considering $\beta = 0$ below rated wind, C_p can be described as a unary function $C_p(\lambda)$, then the small disturbance component of aerodynamic power at operating point OP0 is

$$\begin{cases} \Delta P_a = \mathrm{L}_v|_{OP0}\,\Delta v + \mathrm{L}_\omega|_{OP0}\,\Delta\omega \\ \mathrm{L}_v|_{OP0} = 3k_a C_{p0} v_0^2 - k_a v_0 \omega_B \omega_0 R\ \mathrm{d}C_p/\mathrm{d}\lambda\big|_{\lambda 0} \\ \mathrm{L}_\omega|_{OP0} = k_a \omega_B R v_0^2\ \mathrm{d}C_p/\mathrm{d}\lambda\big|_{\lambda 0} \end{cases} \tag{6}$$

where $\mathrm{L}_v|_{OP0}$, $\mathrm{L}_\omega|_{OP0}$ are P_a's partial derivatives to v, ω at OP0 respectively. For a typical MW scale wind turbine, the peak of $C_p(\lambda)$ curve is very flat, so we can apply $\mathrm{d}C_p/\mathrm{d}\lambda = 0$ to (6) to facilitate the analysis, thus

$$\Delta P_a \approx 3k_a C_{p0} v_0^2 \Delta v \tag{7}$$

The control system of WECS can be divided into central control and converter control. The central controller provides power references for the converter controller. The converter control usually adopts classical vector control or direct

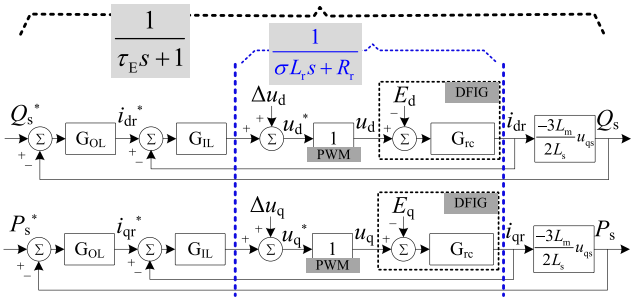

FIGURE 2. Control block of converter control.

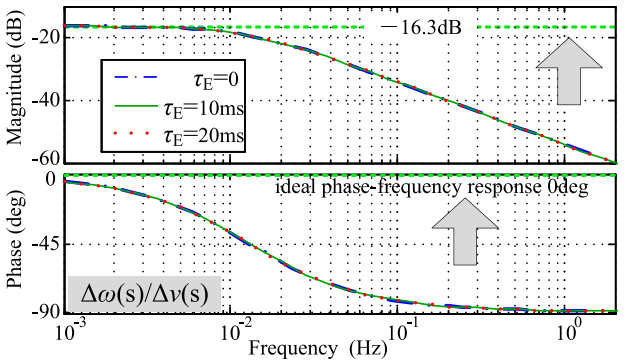

FIGURE 3. Impacts of τ_E on MPPTA (v_0 = 7m/s).

torque/ power control. The converter control and the generator response are illustrated in Fig. 2.

In Fig. 2, i_{dr} and i_{qr} are rotor current in d-q frame, u_d and u_q are port voltage of rotor side converter, u_{qs} is the q-component of grid voltage, '*' represents reference value. G_{OL} is the outer loop (power loop) control, G_{IL} is the inner loop (current loop) control. G_{rc} is the rotor current response of generator. The PLL, PWM module and converter execution is fast enough to represent as '1'. For generator parameters, L_s is the stator inductance, L_r is the rotor inductance, L_m is the mutual inductance, R_r is the rotor resistance. If the decoupling terms (Δu_d and Δu_q) are well designed, the controlled object of inner loop can be expressed as $1/(\sigma L_r s+R_r)$, where σ is the magnetic leakage factor [29]. The converter control together with the generator response has been derived in Appendix, and the external characteristic can be approximated as [30]

$$P_e = \frac{1}{\tau_E s+1} P_e^* \tag{8}$$

τ_E is typically 10 ms with the power electronics techniques.

Then the small signal analysis method will be used to deduce $\Delta\omega(s)/\Delta v(s)$ and $\Delta P_e(s)/\Delta v(s)$.

A. TRADITIONAL OPTIMAL TORQUE CONTROL

The traditional OTC follows (9) or (10)

$$T_e^* = k_{opt}\omega^2 \tag{9}$$

$$P_e^* = k_{opt}\omega^3 \tag{10}$$

where k_{opt} is the optimal torque coefficient. It is dependent on turbine parameters.

$$k_{opt} = 0.5\rho\pi R^5 C_{p\,max}\omega_B^3/(P_B\lambda_{opt}^3) \tag{11}$$

OTC adopts speed opened-loop control. The MPP tracking stability of OTC has been verified in [14]. From (9)- (11),

$$\Delta P_e = \frac{3k_{opt}\omega_0^2}{\tau_E s+1}\Delta\omega \tag{12}$$

Combining (3), (7), (8) and (12), yields

$$\frac{\Delta\omega(s)}{\Delta v(s)} = \frac{3k_a C_{p0} v_0^2(\tau_E s+1)}{J_{sum}\omega_0\tau_E s^2 + J_{sum}\omega_0 s + 3k_{opt}\omega_0^2} \tag{13}$$

Since $\tau_E > 0$ and the poles of $\Delta\omega(s)/\Delta v(s)$ have a negative real part, (13) is another method to verify the stability of OTC.

The impacts of τ_E on MPPTA will be discussed. Taking the real parameter of a 1.5 MW wind turbine [31], three groups of τ_E are chosen, 20ms, 10ms and 0ms, which represents slow response, normal response and ideal response respectively. The results in Fig. 3 show τ_E has tiny impacts on MPPTA (the response of converter and generator are fast enough when compared with the slow dynamics of rotor speed), so we will let $\tau_E = 0$ to simplify the following analysis. This also means PMSG-based WECS and DFIG-based WECS have nearly the same performance on MPPTA and EPF.

Substituting (5) and $\tau_E = 0$, (13) can be rewritten as

$$\frac{\Delta\omega(s)}{\Delta v(s)} = \frac{k_a C_{p0}\omega_B^2 R^2/(k_{opt}\lambda_0^2)}{1 + sJ_{sum}\omega_B R/(3k_{opt}\lambda_0 v_0)} \tag{14}$$

where $C_{p0} = C_{pmax}$, $\lambda_0 = \lambda_{opt}$ and k_{opt} are three constants determined by wind turbine parameters.

Combining (12) and (14), yields

$$\frac{\Delta P_e(s)}{\Delta v(s)} = \frac{3k_a C_{p0} v_0^2}{1 + sJ_{sum}\omega_B R/(3k_{opt}\lambda_0 v_0)} \tag{15}$$

As can be seen, both $\Delta\omega(s)/\Delta v(s)$ and $\Delta P_e(s)/\Delta v(s)$ perform as a first-order low-pass filter, and they share the same filtering time constant τ_{LP}. τ_{LP} is proportional to J_{sum} and inverse proportional to v_0. The gain of transfer function $\Delta\omega(s)/\Delta v(s)$ under different v_0 is constant as λ is kept on λ_{opt} in steady state. The ideal MPPT in region II follows

$$\frac{\omega}{v} = \frac{\lambda_{opt}}{\omega_B R} \tag{16}$$

Thus the ideal AFR of $\Delta\omega(s)/\Delta v(s)$ is $20\log(\lambda_{opt}/(\omega_B R))$, the ideal PFR of $\Delta\omega(s)/\Delta v(s)$ is 0 deg. For the case turbine in this paper, $\lambda_{opt} = 10$, $\omega_B = 1.5$, R = 43.8, the ideal AFR of $\Delta\omega(s)/\Delta v(s)$ yields –16.3 dB.

τ_{LP} determines how $\Delta\omega$ can response to Δv, so τ_{LP} can be used to describe MPPTA, i.e., MPPTA increase with decreasing τ_{LP}. This means MPPTA increase with v_0, or in other words, MPPTA under low wind speed is relatively weak (as shown in Fig. 4a). From (15), the gain of $\Delta P_e(s)/\Delta v(s)$ is proportional to v_0^2, which indicates EPF increase with increasing v_0 (as shown in Fig. 4b).

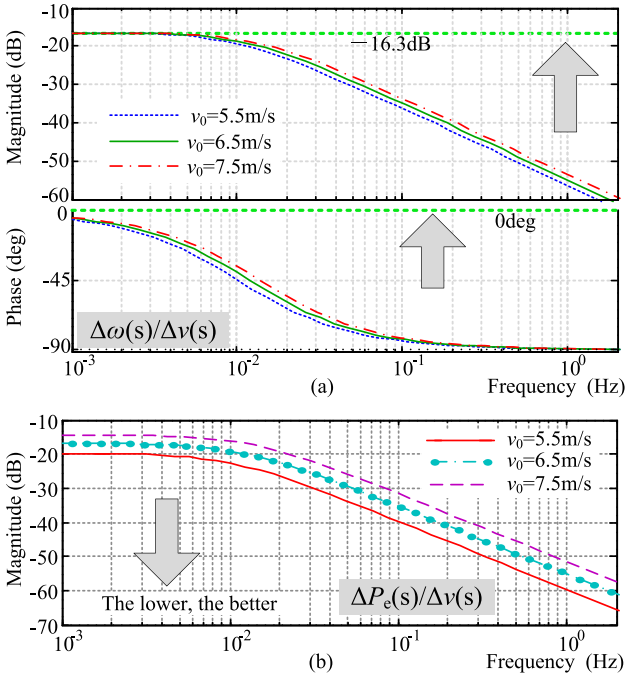

FIGURE 4. Impacts of v_0 on: (a) MPPTA, (b) power fluctuation.

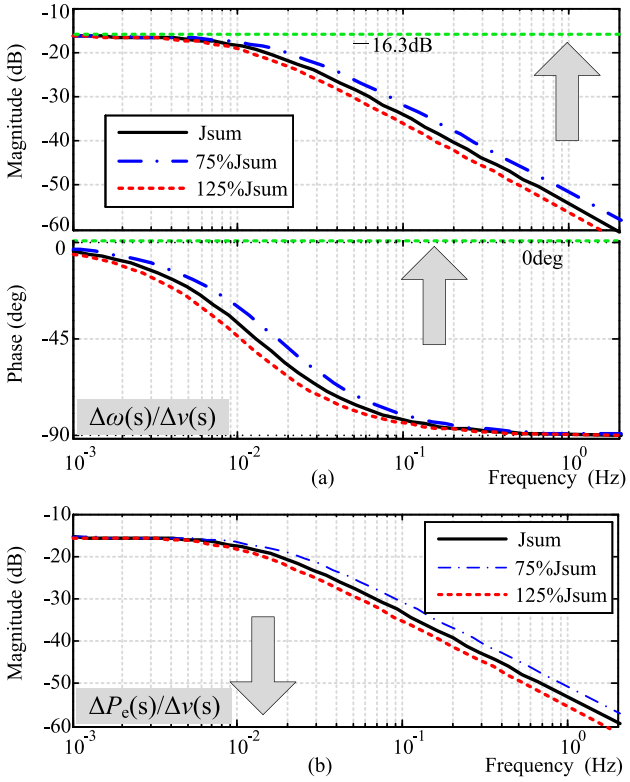

FIGURE 5. Impacts of J_{sum} on: (a) MPPTA, (b) power fluctuation.

Equation (14) indicates the only adjustable variable influencing MPPTA and EPF is J_{sum}. For $\Delta P_e(s)/\Delta v(s)$, the physical significance of τ_{LP} is exactly the power filtering time constant, thus a larger τ_{LP} (and then a lager J_{sum}) is beneficial for power smoothing of WECS. This goes against the requirement of enhancing MPPTA. The impacts of J_{sum} are shown in Fig. 5, in which 'Jsum' adopts the actual parameters of WECS, '75%Jsum' and '125%Jsum' modify J_{sum} accordingly. It shows a smaller J_{sum} is helpful for enhancing MPPTA, while a larger J_{sum} is helpful for lowering EPF. So optimizing J_{sum} is a tradeoff matter.

B. VIRTUAL-INERTIA EMBEDDED OTC

J_{sum} is a determined value for a completed WECS, but we can adjust it virtually through additional generator torque control. So the question is how the virtual inertia contributes to the above mentioned two optimization goals. One of the additional control utilize the derivative of ω,

$$T_e = k_{opt}\omega^2 - J_v\dot{\omega}. \tag{17}$$

Thus,

$$\Delta P_e = (3k_{opt}\omega_0^2 - J_v\omega_0 s)\Delta\omega \tag{18}$$

Combining (3), (7) and (18), yields

$$\frac{\Delta\omega(s)}{\Delta v(s)} = \frac{k_a C_{p0}\omega_B^2 R^2/(k_{opt}\lambda_0^2)}{1 + s(J_{sum} - J_v)\omega_B R/(3k_{opt}\lambda_0 v_0)} \tag{19}$$

$$\frac{\Delta P_e(s)}{\Delta v(s)} = \frac{3k_a C_{p0} v_0^2[1 - sJ_v\omega_B R/(3k_{opt}\lambda_0 v_0)]}{1 + s(J_{sum} - J_v)\omega_B R/(3k_{opt}\lambda_0 v_0)} \tag{20}$$

Since $J_v < J_{sum}$, the pole of (19) has a negative real part, this means the MPP tracking process remains stable when applying (17).

Another additional control adopts the deviation torque between aerodynamic torque and optimal torque [12], [14],

$$T_e = k_{opt}\omega^2 - k_f(\widehat{T}_a - k_{opt}\omega^2). \tag{21}$$

Thus,

$$\Delta P_e = (1 - k_f)3k_{opt}\omega_0^2\Delta\omega - k_f\Delta P_a \tag{22}$$

Combining (3), (7) and (22), yields

$$\frac{\Delta\omega(s)}{\Delta v(s)} = \frac{k_a C_{p0}\omega_B^2 R^2/(k_{opt}\lambda_0^2)}{1 + s\frac{J_{sum}}{1+k_f}\omega_B R/(3k_{opt}\lambda_0 v_0)} \tag{23}$$

Substituting (7) to (22), and combining (23), yields

$$\frac{\Delta P_e(s)}{\Delta v(s)} = 3k_a C_{p0} v_0^2 \frac{1 - s\frac{k_f J_{sum}}{1+k_f}\omega_B R/(3k_{opt}\lambda_0 v_0)}{1 + s\frac{J_{sum}}{1+k_f}\omega_B R/(3k_{opt}\lambda_0 v_0)} \tag{24}$$

One may find (23) is equivalent to (19) and (24) is equivalent to (20) when taking into account (25). This means the two kinds of additional controls are equal, and we will use (19) and (20) to continue the analysis.

$$k_f = J_v/(J_{sum} - J_v) \tag{25}$$

Equation (19) shows J_v is effective in adjusting the low-pass filtering time constant of $\Delta\omega(s)/\Delta v(s)$, i.e., a positive J_v

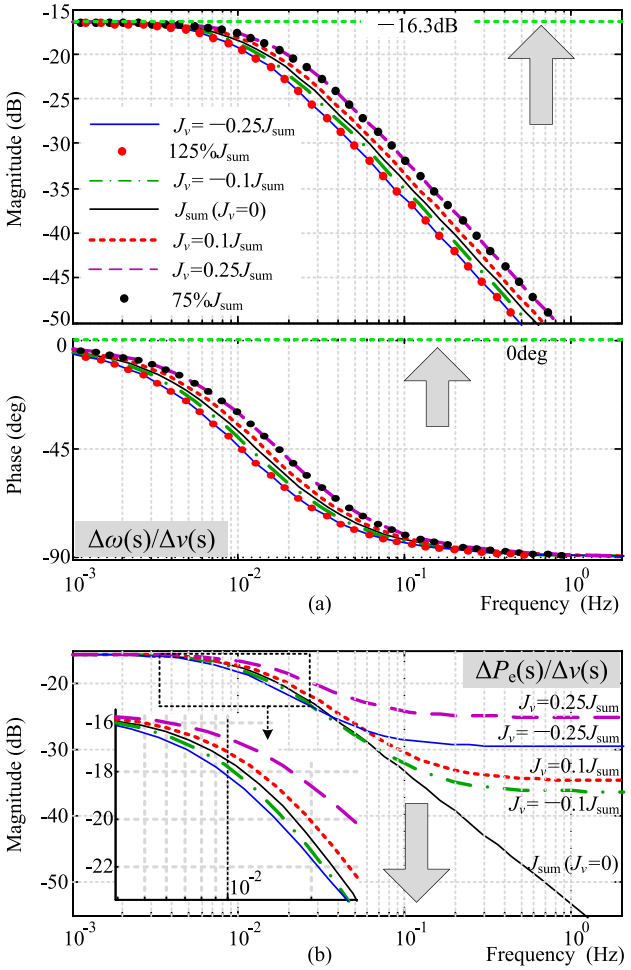

FIGURE 6. Impacts of J_v on: (a) MPPTA, (b) power fluctuation.

will decrease τ_{LP} and thus help increase MPPT performance. But $\Delta P_e(s)/\Delta v(s)$ is no longer a low-pass transfer function, but a lead-lag one. Fig. 6(a) shows that adjusting J_{sum} virtually has the same effect as adjusting real J_{sum} on MPPTA. Fig. 6(b) shows the impacts of J_v on EPF: lowering J_{sum} virtually ($J_v > 0$) will increase EPF in the whole frequency band, while adding J_{sum} virtually ($J_v < 0$) will slightly lower EPF in a low-medium frequency band (0.004 Hz-0.05 Hz) but brings negative effects in the high frequency. This is quite different to the case of adjusting real J_{sum}, and we can draw the conclusion that adjust inertia virtually is harmful to power fluctuation on the whole.

One should also note when adjusting J_{sum} or adjusting J_{sum} virtually, the PFR of $\Delta\omega(s)/\Delta v(s)$ changes in the same direction with AFR. Thus, though it is not so strict for the existing works to evaluate MPPTA with the AFR only, the results are right.

III. ENHANCED OPTIMAL TORQUE CONTROL

A. FREQUENCY_DISTINCT CONTROL

The theoretical analysis in section II shows a smaller J_{sum} benefits power tracking, while a larger J_{sum} benefits power smoothing. And adjust J_{sum} virtually is always harmful to power fluctuation. So the adjustment of J_{sum} can never meet the requirements of power production and power smoothing at the same time.

Since the low frequency component of natural wind contains more energy, enhancing MPPTA in low frequency band is beneficial for power production; on the other hand, enhancing MPPTA for the turbulence component of natural wind may not benefit power production, but do harm to the power fluctuation. So the thought of frequency-distinct control can be introduced to improve the performance of traditional OTC, i.e., frequency-distinct OTC.

To introduce some more changeable factors, we present a modified MPPT control by adding a transfer function $G(s)$ on the traditional strategy, as shown in Fig. 7.

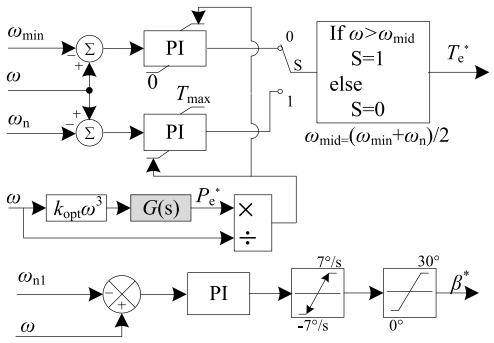

FIGURE 7. The frequency-distinct OTC embedded central controller for overall wind speed operation.

The enhanced torque control equals to the torque control in Fig. 1c if $G(s) = 1$. In region II,

$$\Delta P_e = 3k_{opt}\omega_0^2 G(s)\Delta\omega \tag{26}$$

combining (5), (11) and (34), we get

$$\frac{\Delta\omega(s)}{\Delta v(s)} = \frac{3k_a C_{p0} v_0^2}{J_{sum}\omega_0 s + 3k_{opt}\omega_0^2 G(s)} \tag{27}$$

$$\frac{\Delta P_e(s)}{\Delta v(s)} = \frac{9k_a k_{opt} C_{p0} v_0^2 \omega_0^2 G(s)}{J_{sum}\omega_0 s + 3k_{opt}\omega_0^2 G(s)} \tag{28}$$

Designing $G(s)$ follows the basic rule $|G(j0)| = 1$. This is quite important because $|G(j0)| = 1$ means (27) has the same tracking ability to (14) at low frequency band ($j\omega = j0$), otherwise WECS cannot properly work on MPPT in steady state. The following simple $G(s)$ satisfy this rule

$$G(s) = \frac{1}{1 + \tau s} \tag{29}$$

where τ should be designed to decrease $|\Delta P_e/\Delta v|$ in the interested frequency band. The bode diagram is useful to design such a τ, Fig. 8b shows a reasonable τ is helpful for smoothing EPF on the whole (there is a tradeoff between high frequency band and low frequency band). Substituting (29) into (27), one may find the poles of the characteristic equation

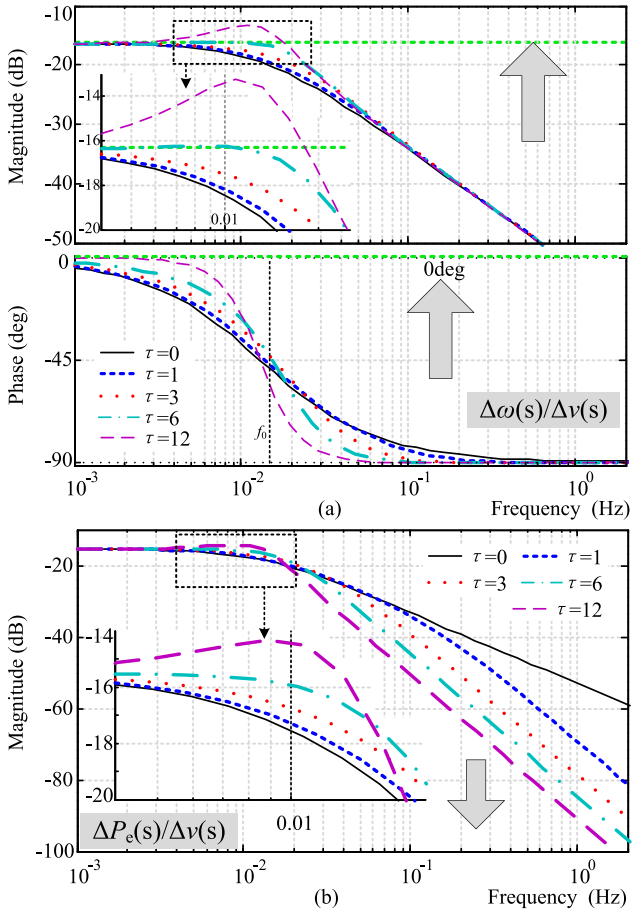

FIGURE 8. The frequency character of enhanced OTC under $v_0 = 7$m/s. (a) $\Delta P_e(s)/\Delta v(s)$. (b) $\Delta\omega(s)/\Delta v(s)$.

always have a negative real part if only $\tau > 0$, this means the MPP tracking process remains stable under frequency-distinct control.

B. A NEW METHOD TO EVALUATE MPPTA

The impacts of τ on MPPTA are shown in Fig. 8(a). From the AFR aspect, a reasonable τ is helpful for MPPTA, while an overlarge τ ($\tau = 12$) should be avoided. One should note the PFR of $\Delta\omega(s)/\Delta v(s)$ no longer change with τ in the same direction with the AFR, which makes it hard to evaluate MPPTA precisely.

To facilitate the design of τ, a new method for MPPTA evaluation is proposed. As C_p is a single-peak function of λ, the basic goal of MPP tracking is to maintain λ_{opt}. Thus $\Delta\lambda(s)/\Delta v(s)$ can be taken as a universal criterion to evaluate MPPTA, in which $\Delta\lambda$ is defined as

$$\Delta\lambda = \lambda - \lambda_{opt} \tag{30}$$

where λ_{opt} is the steady tip speed ratio in region II. $\Delta\lambda(s)/\Delta v(s)$ directly determines the ability to maintain λ_{opt}. The higher C_p is obtained with a smaller $|\Delta\lambda|$, thus the AFR

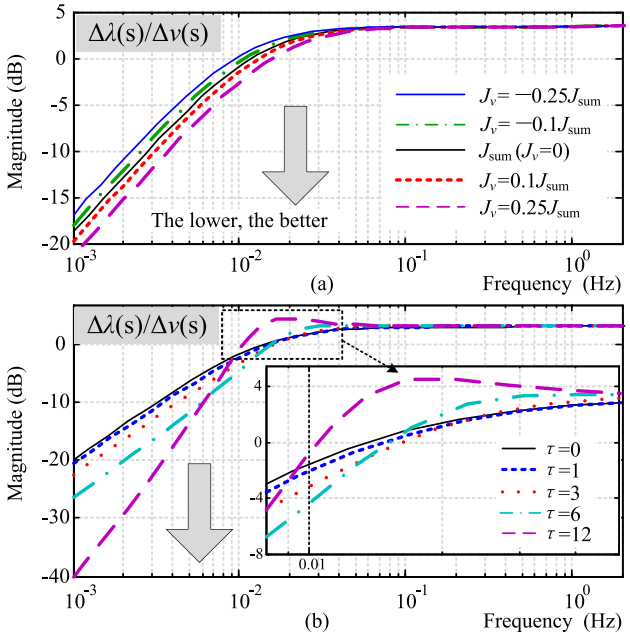

FIGURE 9. The MPPTA evaluation results under $v_0 = 7$m/s based on $\Delta\lambda(s)/\Delta v(s)$. (a) OTC with virtually adjusted J_{sum}. (b) Frequency-distinct OTC.

is enough to judge MPPTA. From (5),

$$\Delta\lambda = \omega_B R(\frac{1}{v_0}\Delta\omega - \frac{\omega_0}{v_0^2}\Delta v) = \lambda_{opt}(\frac{\Delta\omega}{\omega_0} - \frac{\Delta v}{v_0}) \tag{31}$$

For OTC with virtually adjusted J_{sum}, substituting (19) to (31) yields

$$\frac{\Delta\lambda}{\Delta v} = \lambda_{opt}\frac{-(J_{sum} - k_v)\omega_0^2 s + 3k_a C_{p0} v_0^3 - 3k_{opt}\omega_0^3}{(J_{sum} - k_v)v_0\omega_0^2 s + 3k_{opt}v_0\omega_0^3} \tag{32}$$

considering $C_{p0} = C_{pmax}$, we get $3k_a C_{p0} v_0^3 = 3k_{opt}\omega_0^3$. Thus

$$\frac{\Delta\lambda}{\Delta v} = \lambda_{opt}\frac{-(J_{sum} - k_v)\omega_0^2 s}{(J_{sum} - k_v)v_0\omega_0^2 s + 3k_{opt}v_0\omega_0^3} \tag{33}$$

For frequency-distinct OTC, substituting (19) to (31) yields

$$\frac{\Delta\lambda}{\Delta v} = \lambda_{opt}\frac{-J_{sum}\omega_0^2\tau s^2 + (3k_a C_{p0} v_0^3\tau - J_{sum}\omega_0^2)s}{J_{sum}v_0\omega_0^2\tau s^2 + J_{sum}v_0\omega_0^2 s + 3k_{opt}v_0\omega_0^3} \tag{34}$$

As rotor speed can hardly respond (i.e., $\Delta\omega = 0$) to high-frequency fluctuating Δv, from (31) we get the ideal AFR of $\Delta\lambda(s)/\Delta v(s)$ at high frequency band is $20*\log(\lambda_{opt}/v_0)$. When $v_0 = 7$m/s, it yields 3.1 dB. For virtual-inertia embedded OTC, the MPPTA evaluation results are shown in Fig. 9(a). It shows a monotonic impact of J_v, which is in accordance with the same-direction-influence of AFR and PFR of $\Delta\omega(s)/\Delta v(s)$. For frequency-distinct OTC (see Fig. 9(b)), the reverse-direction-influence of AFR and PFR of $\Delta\omega(s)/\Delta v(s)$ cause the AFR of $\Delta\lambda(s)/\Delta v(s)$ a little complex, but it is still easy to design the appropriate τ ($\tau = 6$ for the WECS in this paper).

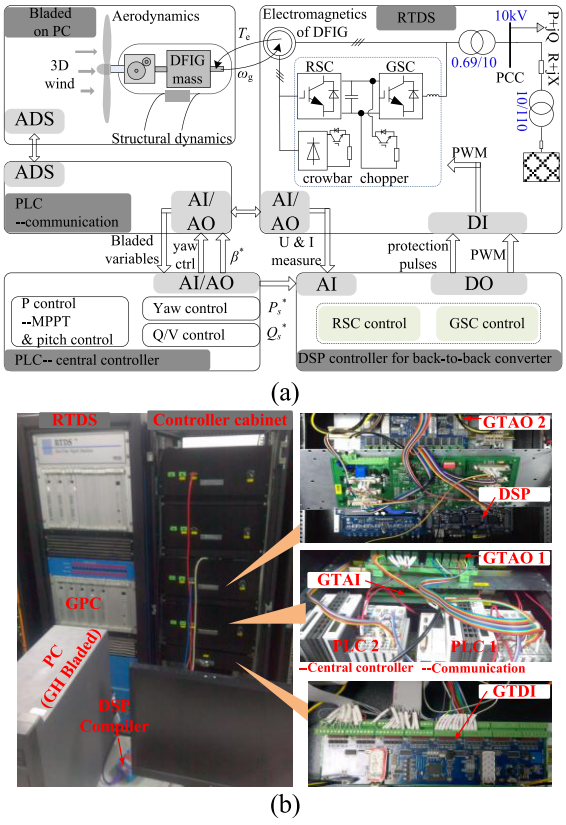

FIGURE 10. Refined simulation platform based on RTDS and Bladed. (a) Schematic diagram. (b) Experimental devices.

IV. SIMULATION VERIFICATIONS

The analysis results are verified with the real time co-simulation platform based on real time digital simulator (RTDS) and GH Bladed, as shown in Fig. 10. GH Bladed is a professional simulation package for wind turbine design. RTDS is a powerful simulator for electromagnetic transient. On the basis of interfacing technique, the wind model, aerodynamics model and structural dynamics model were built in Bladed, while the electrical parts of the WECS was built in RTDS, so the co-simulation platform fits the demand of refined simulation quite well [31].

A. VERIFICATION OF J_{sum} ADJUSTMENT

Different schemes of J_{sum} adjustment are simulated under the wind speed in Fig. 11(a). The mean wind speed at the beginning and the end are the same, so that the rotational kinetic energy at the beginning and the end are the same, and the aerodynamic power captured by wind turbine are converted to electric power completely. Thus the power production, which is the integral of P_{e}, could be used to evaluate the effects of MPPTA. The power smoothing factor (PSF) is defined to evaluate the power smoothing effects.

$$\text{PSF} = \int (|\dot{P}_{\text{e}}|/P_{\text{n}})\text{d}t \tag{35}$$

In Fig. 11, the label 'J_{sum}' represents traditional OTC with no adjustment on rotor inertia. '$1.25J_{\text{sum}}$', '$J_{\text{v}} = -0.25J_{\text{sum}}$' represents add $0.25J_{\text{sum}}$ and virtually add $0.25J_{\text{sum}}$ respectively. It shows the additional J_{sum} slower the response of rotor speed towards its new steady state. As the same J_{sum} is added, '$1.25J_{\text{sum}}$' and '$J_{\text{v}} = -0.25J_{\text{sum}}$' have nearly the same rotor speed response, but the electric power are quite different in the acceleration stage and the deceleration stage. During the steady state in 85s to 120s, 'add real inertia' lower the EPF, while 'add inertia virtually' increase the EPF. Both

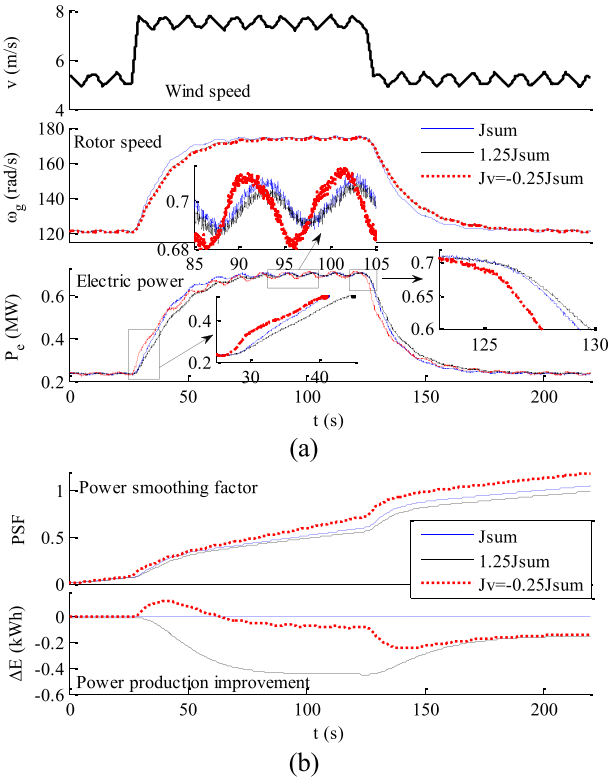

FIGURE 11. Simulation results of gaining J_{sum}. (a) Wind speed, generator speed and electric power. (b) PSF and power production improvement.

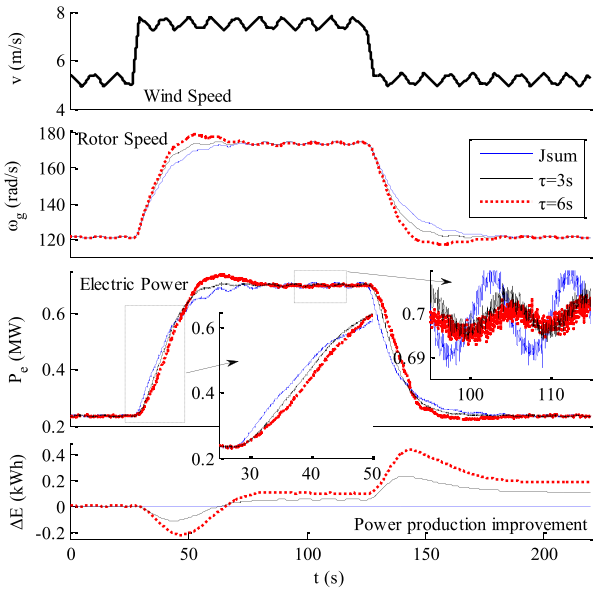

FIGURE 12. Simulation results of frequency-distinct OTC.

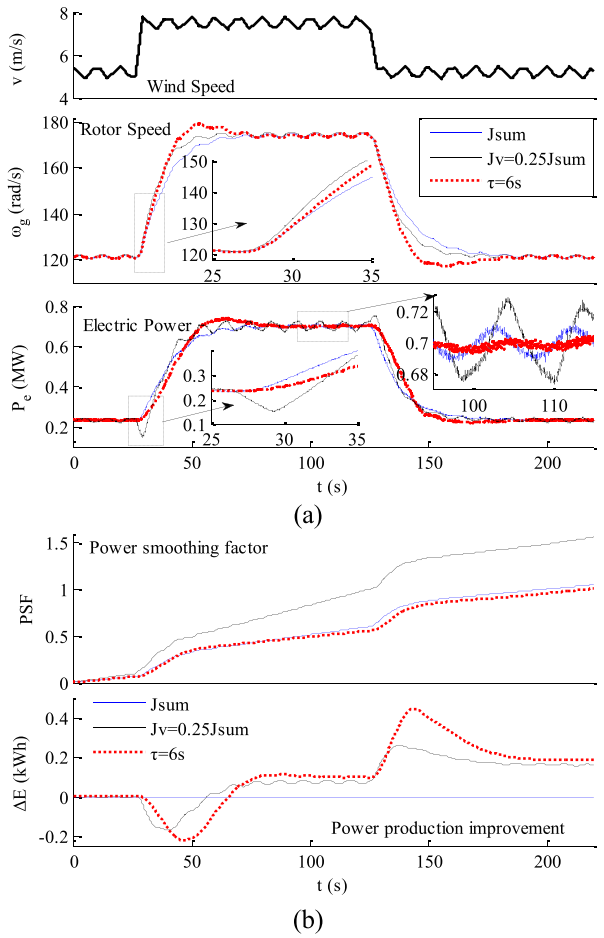

FIGURE 13. Comparison of frequency-distinct OTC and OTC embedded with virtual-lowering J_{sum}.

of the additional J_{sum} schemes lose some power production due to the deteriorated MPPTA. These results are in consistent with the analysis.

B. VERIFICATION OF FREQUENCY-DISTINCT OTC

G(s) with different filter time constant τ are compared in Fig. 12. It shows when applying frequency-distinct control, the generator speed response faster in the acceleration stage and the deceleration stage, which means the MPPTA is enhanced. During the steady state in 90s to 120s, the electric power fluctuation caused by varying wind speed is smoothed. When compared to 'J_{sum}', the power production of '$\tau = 3$s' and '$\tau = 6$s' increased by 0.11kWh and 0.195kWh respectively.

C. ADVANTAGES OF FREQUENCY-DISTINCT OTC

The existing method for enhancing MPPTA reduces the inertia of WECS virtually through generator control. A group of simulation is done under the same wind speed, in which '$J_v = 0.25J_{sum}$' represents the inertia is reduced virtually by $0.25J_{sum}$ to enhance the MPPTA, '$\tau = 6$s' represents frequency-distinct OTC. The simulation results in Fig. 13 shows the MPPTA is enhanced effectively in both schemes. When applying '$J_v = 0.25J_{sum}$', the wind steps cause a sharp varying on electric power, and the power fluctuation is seriously deteriorated in steady state. Fig. 13(b) shows the power production improvement is comparative, while the PSFs are quite different. This shows the advantages of the proposed frequency-distinct control.

V. CONCLUSION

Improving power production and power smoothing are two important optimization goals for WECS control. The maximum power point tracking ability and power fluctuation characteristics are analyzed in frequency domain with small signal analysis method. The analysis indicates J_{sum} adjustment, either adjust real J_{sum} or adjust J_{sum} virtually, can never meet the requirements of power production and power smoothing at the same time.

A frequency-distinct OTC approach is proposed to deal with this problem, which not only enhances the MPPTA in low frequency band to improve power production, but also reduces the power fluctuations caused by high frequency wind speed. The transfer function $\Delta\lambda(s)/\Delta v(s)$ is defined as a universal criterion to evaluate MPPTA, which facilitate the parameter design of the proposed control strategy. The effects of power production improvement and power smoothing are fully verified by refined co-simulation.

APPENDIX

From Fig. 2,

$$G_{IL} = \frac{k_{pI}s + k_{iI}}{s} \tag{A-1}$$

$$G_{OL} = \frac{k_{pO}s + k_{iO}}{s} \tag{A-2}$$

$$G_G = \frac{1}{\sigma L_r s + R_r} \tag{A-3}$$

The q-axis rotor current response to its reference,

$$\frac{i_{qr}(s)}{i^*_{qr}(s)} = \frac{G_{IL}G_G}{1 + G_{IL}G_G} = \frac{k_{pI}s + k_{iI}}{\sigma L_r s^2 + (R_r + k_{pI})s + k_{iI}} \tag{A-4}$$

The active power response to its reference of generator stator,

$$\frac{P_s(s)}{P^*_s(s)} = \frac{\text{den}(s)}{\sigma L_r s^3 + (R_r + k_{pI})s^2 + k_{iI}s + \text{den}(s)}$$

$$\text{den}(s) = 1.5\frac{L_m u_{qs}}{L_s}[k_{pO}k_{pI}s^2 + (k_{pO}k_{iI} + k_{pI}k_{iO})s + k_{iO}k_{iI}] \tag{A-5}$$

Since G_{IL} has a much higher control bandwidth than G_{OL},

$$\frac{P_s(s)}{P^*_s(s)} \approx \frac{1}{\tau s + 1} \tag{A-6}$$

REFERENCES

[1] *Renewables 2016 Global Status Report*, REN21, Paris, France, 2014. [Online]. Available: http://www.ren21.net

[2] M. Said, M. El-Shimy, and M. A. Abdelraheem, "Improved framework for techno-economical optimization of wind energy production," *Sustain. Energy Technol. Assessments*, vol. 23, pp. 57–72, Oct. 2017.

[3] Y. Ma, W. Cao, L. F. Yang, F. Wang, and L. M. Tolbert, "Virtual synchronous generator control of full converter wind turbines with short-term energy storage," *IEEE Trans. Ind. Electron.*, vol. 64, no. 11, pp. 8821–8831, Nov. 2017.
[4] E. A. Bossanyi, "The design of closed loop controllers for wind turbines," *Wind Energy*, vol. 3, no. 3, pp. 149–163, Sep. 2000.
[5] J. P. Ram, N. Rajasekar, and M. Miyatake, "Design and overview of maximum power point tracking techniques in wind and solar photovoltaic systems: A review," *Renew. Sustain. Energy Rev.*, vol. 73, pp. 1138–1159, Jun. 2017.
[6] Y. Xia, K. H. Ahmed, and B. W. Williams, "A new maximum power point tracking technique for permanent magnet synchronous generator based wind energy conversion system," *IEEE Trans. Power Electron.*, vol. 26, no. 12, pp. 3609–3620, Dec. 2011.
[7] M. N. Uddin and N. Patel, "Maximum power point tracking control of IPMSG incorporating loss minimization and speed sensorless schemes for wind energy system," *IEEE Trans. Ind. Appl.*, vol. 52, no. 2, pp. 1902–1912, Mar. 2016.
[8] J. Liu, Y. Gao, S. Geng, and L. Wu, "Nonlinear control of variable speed wind turbines via fuzzy techniques," *IEEE Access*, vol. 5, pp. 27–35, Aug. 2016.
[9] T. D. Do, "Disturbance observer-based fuzzy SMC of WECSs without wind speed measurement," *IEEE Access*, vol. 5, pp. 147–155, Nov. 2016.
[10] D. Song, Y. Yang, M. Su, A. Liu, Y. Liu, and Y. H. Joo, "A comparison study between two MPPT control methods for a large variable-speed wind turbine under different wind speed characteristics," *Energies*, vol. 10, no. 5, p. 613, May 2017.
[11] S. M. R. Kazmi, H. Goto, H.-J. Guo, and O. Ichinokura, "Review and critical analysis of the research papers published till date on maximum power point tracking in wind energy conversion system," in *Proc. IEEE ECCE*, Sep. 2010, pp. 4075–4082.
[12] K. Yenduri and P. Sensarma, "Maximum power point tracking of variable speed wind turbines with flexible shaft," *IEEE Trans. Sustain. Energy*, vol. 7, no. 3, pp. 956–965, Jan. 2016.
[13] J. Chen, J. Chen, and C. Gong, "New overall power control strategy for variable-speed fixed-pitch wind turbines within the whole wind velocity range," *IEEE Trans. Ind. Electron.*, vol. 60, no. 7, pp. 2652–2660, Jul. 2013.
[14] K. E. Johnson, L. J. Fingersh, M. J. Balas, and L. Y. Pao, "Methods for increasing region 2 power capture on a variable-speed wind turbine," *J. Solar Energy Eng.*, vol. 126, no. 4, pp. 1092–1100, Nov. 2004.
[15] J. Chen, J. Chen, and C. Gong, "Constant-bandwidth maximum power point tracking strategy for variable-speed wind turbines and its design details," *IEEE Trans. Ind. Electron.*, vol. 60, no. 11, pp. 5050–5058, Nov. 2013.
[16] K.-H. Kim, T. L. Van, D.-C. Lee, S.-H. Song, and E.-H. Kim, "Maximum output power tracking control in variable-speed wind turbine systems considering rotor inertial power," *IEEE Trans. Ind. Electron.*, vol. 60, no. 8, pp. 3207–3217, Aug. 2013.
[17] A. B. Attya and T. Hartkopf, "Wind turbine contribution in frequency drop mitigation—Modified operation and estimating released supportive energy," *IET Generat. Transmiss. Distrib.*, vol. 8, no. 5, pp. 862–872, May 2014.
[18] C. Luo, H. Banakar, B. Shen, and B.-T. Ooi, "Strategies to smooth wind power fluctuations of wind turbine generator," *IEEE Trans. Energy Convers.*, vol. 22, no. 2, pp. 341–349, Jun. 2007.
[19] A. H. Kasem, E. F. El-Saadany, H. H. El-Tamaly, and M. A. A. Wahab, "Power ramp rate control and flicker mitigation for directly grid connected wind turbines," *IET Renew. Power Generat.*, vol. 4, no. 3, pp. 261–271, May 2010.
[20] Y. J. Li and Z. Xu, "Power smoothing control of wind turbines using different strategies," in *Proc. IEEE Int. Conf. Smart Grid Commun.*, Nov. 2016, pp. 705–710.
[21] N. K. S. Naidu and B. Singh, "Grid-interfaced DFIG-based variable speed wind energy conversion system with power smoothening," *IEEE Trans. Sustain. Energy*, vol. 8, no. 1, pp. 51–58, Jan. 2017.
[22] N. S. Gayathri, N. Senroy, and I. N. Kar, "Smoothing of wind power using flywheel energy storage system," *IET Renew. Power Generat.*, vol. 11, no. 3, pp. 289–298, Apr. 2017.
[23] Y. Kim, M. Kang, E. Muljadi, J. W. Park, and Y. C. Kang, "Power smoothing of a variable-speed wind turbine generator in association with the rotor speed-dependent gain," *IEEE Trans. Sustain. Energy*, vol. 8, no. 3, pp. 990–1000, Jul. 2017.
[24] B. G. Rawn, P. W. Lehn, and M. Maggiore, "Control methodology to mitigate the grid impact of wind turbines," *IEEE Trans. Energy Convers.*, vol. 22, no. 2, pp. 431–438, Jun. 2007.
[25] B. G. Rawn, P. W. Lehn, and M. Maggiore, "Disturbance margin for quantifying limits on power smoothing by wind turbines," *IEEE Trans. Control Syst. Technol.*, vol. 21, no. 5, pp. 1795–1807, Sep. 2013.
[26] X. X. Zhao, Z. H. Yan, Y. Xue, and X. P. Zhang, "Wind power smoothing by controlling the inertial energy of turbines with optimized energy yield," *IEEE Access*, vol. 5, pp. 23374–23382, Sep. 2017.
[27] J. Liu, H. Meng, Y. Hu, Z. Lin, and W. Wang, "A novel MPPT method for enhancing energy conversion efficiency taking power smoothing into account," *Energy Convers. Manage.*, vol. 101, pp. 738–748, Sep. 2015.
[28] T. Burton, N. Jenkins, D. Sharpe, and E. A. Bossanyi, *Wind Energy Handbook*, 2nd ed. New York, NY, USA: Wiley, 2011, pp. 9–16.
[29] T. Sun, "Power quality of grid-connected wind turbines with DFIG and their interaction with the grid," Ph.D. dissertation, Dept. Inst. Energy Technol., Aalborg Univ., Aalborg, Denmark, Sweden, 2004.
[30] M. Soliman, O. P. Malik, and D. T. Westwick, "Multiple model predictive control for wind turbines with doubly fed induction generators," *IEEE Trans. Sustain. Energy*, vol. 2, no. 3, pp. 215–225, Jul. 2011.
[31] F. Jia, X. Cai, Y. Lou, and Z. Li, "Interfacing technique and hardware-in-loop simulation of real-time co-simulation platform for wind energy conversion system," *IET Generat. Transmiss. Distrib.*, vol. 11, no. 12, pp. 3030–3038, Sep. 2017.

FENG JIA received the M.Eng. degree in power electronics and power drives from the China University of Mining and Technology, Jiangsu, China, in 2013. He is currently pursuing the Ph.D. degree in electrical engineering from Shanghai Jiao Tong University, Shanghai, China.

His current interests include the modeling and control of wind energy conversion system.

XU CAI received the B.Eng. degree from Southeast University, Nanjing, China, in 1983, and the M.Sc. and Ph.D. degrees from the China University of Mining and Technology, Jiangsu, China, in 1988 and 2000, respectively.

He was with the Department of Electrical Engineering, China University of Mining and Technology, as an Associate Professor, from 1989 to 2001. In 2002, he joined Shanghai Jiao Tong University, as a Professor. In 2008, he was a Director of the Wind Power Research Center, Shanghai Jiao Tong University. He was a Vice Director of the State Energy Smart Grid R&D Center, Shanghai, from 2010 to 2013. His special fields of interest lie in power electronics and renewable energy exploitation and utilization, including wind power converters, wind turbine control system, large power battery storage systems, and clustering of wind farms and its control system and grid integration.

ZHENG LI received the B.Eng. and M.Eng. degrees in electrical engineering from Southeast University, Nanjing, China, in 1983 and 1986, respectively, and the Ph.D. degree in control science and engineering from Donghua University, Shanghai, China, in 1999. From 2005 to 2006, she was with the Department of Aalborg University, Denmark, as a Visiting Researcher.

Since 1986, she has been with the Department of Electrical Engineering and its Automation, Donghua University, as an Assistant Professor, an Associate Professor, and then a Professor, in 2007. She was a Vice Dean and a Professor of the School of Information Science and Technology, Donghua University, from 2002 to 2007. She is currently a Deputy Dean of the School of Environment Science and Engineering, Donghua University. Her research interests lie in the field of distributed renewable energy system and its integration, energy storage systems, intelligent control system, and hybrid systems control.